Modeling of Oligomeric-State Dependent Spectral Heterogeneity in the B875 Light-Harvesting Complex of *Rhodobacter sphaeroides* by Numerical Simulation

Willem H. J. Westerhuis,[†] C. Neil Hunter,[†] Rienk van Grondelle,[‡] and Robert A. Niederman*[,§]

Department of Molecular Biology and Biotechnology, University of Sheffield, Sheffield S10 2TN, U.K., Department of Biophysics, Faculty of Physics and Astronomy, Free University, De Boelelaan 1081, 1081 HV Amsterdam, The Netherlands, and Department of Molecular Biology and Biochemistry, Rutgers University, Piscataway, New Jersey 08854-8082

Received: June 3, 1999; In Final Form: July 21, 1999

A series of detergent-isolated light-harvesting 1 (LH1, B875) complexes from *Rhodobacter sphaeroides*, estimated to range in size from $(\alpha\beta BChl_2)_4$ to $(\alpha\beta BChl_2)_{13}$, was used to study the combined effects of spectral disorder and excitonic interactions on oligomeric-state dependent optical properties. Numerical simulations of absorption and fluorescence emission, excitation, and polarization spectra, based on the structure of the related LH2 complex, were compared to spectra measured experimentally at 77 K (Westerhuis and Niederman, in preparation). The aggregation-state dependence of the polarization spectra was found to be particularly sensitive to the choice of parameters, and vibronic components were included to obtain satisfactory simulations. Good agreement with most experimental features, including the oligomeric-state dependence of the absorption and emission maxima, was obtained only when the inter- and intradimer coupling strengths for adjacent BChls were similar (200−260 cm^{-1}), and the width for the inhomogeneous distribution function (300−400 cm^{-1}) was comparable. The relevance of these findings to existing controversies on the physical origin of spectral heterogeneity observed for the LH1 complex is discussed.

Introduction

The LH1 (B875) complex of the proteobacterium *Rhodobacter sphaeroides* functions as a core antenna that collects excitations from the peripheral LH2 (B800−850) antenna and transfers them to photosynthetic reaction centers which it surrounds and interconnects.[1,2] (LH1 and LH2 are core and peripheral light-harvesting complexes, designated respectively as B875 and B800−850 on the basis of near-IR absorbance maxima.) In previous studies,[3,4] we described the isolation and characterization of an oligomeric series of LH1 complexes by lithium dodecyl sulfate−polyacrylamide gel electrophoresis that exhibited oligomeric-state dependent optical properties at 77 K.[3] The various LH1 gel bands differed in size by a single $\alpha\beta$-heterodimeric unit[4] and exhibited blue shifts in absorption and fluorescence emission maxima, as well as pronounced increases in fluorescence polarization with decreased cluster size.[3] These properties were originally ascribed to excitonic coupling of B875 BChl (bacteriochlorophyll *a*), organized into curvilinear arrays.[5] In the present paper, the recently determined structures of two LH2 complexes have formed a basis for the reevaluation of alternative models to explain the origin of spectral inhomogeneity within this strongly coupled light-harvesting complex.

A high-resolution X-ray structure was first elucidated for the LH2 complex of *Rhodopseudomonas acidophila*,[6] which was shown to form a ringlike assembly with the transmembrane α helices of 9 β and 9 α apoproteins making up the respective outer and inner walls. A continuous overlapping ring of 18 B850 BChl molecules is sandwiched between them, while the nine B800 BChls are positioned on the outer surface between the β-polypeptide helices. Carotenoid molecules were found intertwined with the phytol chains of the BChls, spanning most of the membrane. A similar structure with 8 α and β units was determined for the LH2 complex of *Rhodospirillum molischianum*,[7] whereas the LH2 complex of *R. sphaeroides* consists of an $(\alpha\beta)_9$ ring.[8] The LH1 complex of *Rhodospirillum rubrum* also forms a ringlike structure composed of 16 $\alpha\beta$ heterodimers enclosing an overlapping ring of 32 BChls, based upon an electron diffraction analysis of two-dimensional crystals.[9] A similar arrangement is likely for the *R. sphaeroides* LH1 complex.[8]

A number of new insights on the mechanisms of energy migration, the extent to which excitation energy is delocalized over chromophore rings, and the physical origin of spectral inhomogeneity have arisen from these significant structural advances (reviewed in refs 10 and 11). Spectral inhomogeneity was first observed in the *R. sphaeroides* LH1 complex as an increase in fluorescence polarization upon selective excitation in the red wing of the Q_y (875 nm) absorption band,[12,13] and subsequently by measurements of fast absorption changes[14] and energy equilibration dynamics.[15,16] Although attributed originally to a distinct long-wavelength subantenna, designated as B896,[13] multiphasic fluorescence decay kinetics[17] suggested that spectral heterogeneity within the LH1 absorption band is considerably more complex and arises from equilibration of excitations over an inherently inhomogeneous lattice of pigment molecules. Moreover, the dependence of both the emission maximum and fluorescence polarization on excitation wavelength as determined from site-selection fluorescence measurements[18] was explained by inhomogeneous band broadening. This could result from spectrally inhomogeneous clusters of strongly coupled BChl dimers with small, random differences in local pigment environ-

* To whom correspondence should be addressed. Phone: (732) 445-3985. Fax #: (732) 445-4213. E-mail: rniederm@rci.rutgers.edu.
[†] University of Sheffield.
[‡] Free University Amsterdam.
[§] Rutgers University.

10.1021/jp991816t CCC: $18.00
Published on Web 08/20/1999

ments that transfer energy via the hopping of localized excitations; anisotropic fluorescence would arise from selective excitation of the lowest energy sites within a complex. Excitonic coupling within such BChl dimers was suggested from the optical properties of the B820 subunit form of LH1,[19−21] believed to consist of a single $\alpha\beta$-heterodimeric structural unit.[22,23]

Alternatively, from hole burning experiments, spectral inhomogeneity was proposed[24−26] to arise from a long-wavelength species representing the lowest energy component of an excitonically coupled chromophore aggregate. The anisotropy of such a long-wavelength component, as well as the magnitude of bleaching per absorbed light quantum, has been attributed to strong excitonic coupling within a circular array of chromophores[27] and has also been proposed to explain the oligomerization state-dependent optical properties of the LH1 complex.[5] Further support for delocalization of excitation energy over more than a single BChl dimer comes from ps absorption difference measurements on LH1[28] and LH2.[29,30] This would appear to be confirmed by the organization of B850 BChls into a circular array with pigments on neighboring units in close proximity, as revealed by the detailed molecular architecture of LH2.[6,7]

Recent crystal structure-based calculations[31,32] have also suggested that interchromophore interaction energies lead to significant excitonic coupling, accounting for approximately half of the ∼80 nm red shift of the absorption band. The remaining ∼40 nm arises from pigment−protein interactions, in part to C_2-acetyl hydrogen bonds provided by two Tyr residues;[33] when eliminated by site-directed mutagenesis, the absorption red shift was reduced by ∼25 nm.[34] Analogous mutagenesis studies on the LH1 complex[35] supported a similar relationship between structure and optical properties for both LH2 and LH1.

While these calculations did not take site-inhomogeneity into account, disorder was included in recent numerical simulations,[36] where excitons were estimated to be delocalized over approximately five chromophores. Contributions by phonons resulted in additional localization, and incoherent hopping among BChl dimers provided an adequate explanation for excitation energy migration at 300 K. At this temperature, energy was estimated to be delocalized over $\leq 4 \pm 2$ BChls for both LH2 and LH1, by fitting equilibrated sub-ps transient absorption difference spectra to an excitonic model.[37−39] Superradiance measurements of LH2 and LH1[40] also showed localization of excitations at 300 K and support the idea that inhomogeneity of site energies strongly reduces exciton delocalization length even where relatively strong interdimer interactions exist.[10] It should also be noted that considerably larger values have been estimated for delocalization length in LH2[6] and that delocalization is thought to be time-dependent.

At lower temperatures, delocalization increases for LH1 but not for LH2, indicating that ratios between inhomogeneous broadening and coupling strength may differ. Extensive delocalization occurs only in regular one-dimensional aggregates when this ratio is below unity,[41] but others[25,26,42] contend that the disorder is too small to lead to a significant localization. However, a fit of the CD spectrum of the B850 band in a *R. sphaeroides* mutant without B800 was recently made[43] using estimates of intra- and interdimer interaction energies of ∼300 cm^{-1} and ∼230 cm^{-1}, respectively, taking into account an intrinsic disorder of 500 cm^{-1} and a homogeneous line width of 200 cm^{-1}; these parameters support a localized character for excitons in LH2. Moreover, the red shift of CD crossing relative to OD maximum could be explained only by assuming different diagonal energies for α and βB850 BChls (see also refs 44 and 45).

Here, aggregation-state dependent optical properties of an oligomeric LH1 series,[3] representing ring fragments of 4 to 13 $\alpha\beta(BChl)_2$ heterodimers,[4] were numerically simulated to assess relative contributions of disorder and excitonic interaction to observed spectral inhomogeneity. By varying site inhomogeneity and interdimer coupling strengths, different relationships between spectral properties and cluster size were obtained. Satisfactory fits to observed spectra were achieved with a model in which the width of the inhomogeneous distribution of monomer site energies was comparable to the magnitudes of intra- and interdimer interaction energies. The relevance of these findings to existing controversies is discussed.

Computation Methods

Computations of excitonic components resulting from all interactions among a set of transition dipoles were performed by using software developed and kindly provided by Dr. F. van Mourik, at Free University, Amsterdam, The Netherlands. This program was adapted for analyses of circular pigment dimer arrays having different intra- and inter-unit geometries, with static disorder in monomer site energies given by an inhomogeneous distribution function; it was expanded with routines to generate absorption ($A(\lambda)$) and fluorescence emission ($F(\lambda)$) spectra. These were obtained by summation of the excitonic components (i) convoluted with a Gaussian envelope centered at λ_i, representing the homogeneous band shape $A_i(\lambda)$; for emission spectra, the same components were weighted by a Boltzmann factor prior to summation and rescaled to unit total fluorescence yield. Components that together contributed less than 2% to the absorption spectrum were omitted to reduce computation time

$$A(\lambda) = \sum_i A_i(\lambda) \tag{1a}$$

$$F(\lambda) = \sum_j F_j(\lambda) \tag{1b}$$

with

$$F_j(\lambda) = A_j(\lambda)\exp(-h\nu j/kT)/\int(\sum_j A_j(\lambda)\exp(-h\nu j/kT)\mathrm{d}\lambda \tag{1c}$$

where the frequency of the lowest energy excitation level is defined as zero.

To generate fluorescence excitation and polarization spectra, the experimental conditions were mimicked by multiplying each of the fluorescence components (j) with a 10-nm full bandwidth at half maximum (fwhm) wide Gaussian ($\Omega(\lambda)$) centered at the low energy side of the emission band, representing the optical filter through which fluorescence was detected. This yielded the relative contribution (weight W_j) of the various fluorescing transition dipoles to the measurement

$$W_j = \int F_j(\lambda)\Omega(\lambda)\mathrm{d}\lambda \tag{2}$$

Excitation ($E(\lambda)$) and anisotropy ($Ay(\lambda)$) spectra for right-angle detection were then determined as

$$E(\lambda) = (\sum_j W_j)A(\lambda) \quad (3a)$$

$$A_y(\lambda) = \{\sum_j W_j \sum_i A_i(\lambda)(3\cos^2 \alpha_{ij} - 1)/5\}/E(\lambda) \quad (3b)$$

where indices i and j denote absorbing and fluorescing spectral components, respectively, and α_{ij} the angle between the corresponding transition dipoles.

Disorder was included by adding a random deviation, distributed as a Gaussian (inhomogeneous distribution function), to the monomer site energies and averaging the absorption, emission, excitation, and anisotropy spectra for 500−5000 (N) individual solutions (k)

$$A(\lambda) = \sum_{k=1}^{N} A^k(\lambda) \quad F(\lambda) = \sum_{k=1}^{N} F^k(\lambda) \quad E(\lambda) = \sum_{k=1}^{N} E^k(\lambda) \quad (4a)$$

$$A_y(\lambda) = \{\sum_{k=1}^{N} A_y{}^k(\lambda)E^k(\lambda)\}/E(\lambda) \quad (4b)$$

To facilitate comparison with experimental results, anisotropy spectra were expressed in terms of polarization ($p(\lambda) = 3Ay(\lambda)/(Ay(\lambda) + 2)$). For simplicity, disorder was considered for diagonal elements only, since disorder in the nondiagonal elements is expected to be less important.

Results

Polarized Fluorescence from Circular Pigment Arrays. The experimentally observed dependence of fluorescence polarization spectra on the aggregation state, obtained with a series of LH1 complexes isolated by lithium dodecyl sulfate−polyacrylamide gel electrophoresis,[3] is shown in Figure 1. The gradual decrease in the average polarization value across the absorption band with increasing oligomer size supports the hypothesis that the various bands consist of partial rings or arcs arising from a circular array analogous to LH2.[6] All Q_y transitions would have predominantly parallel orientations, while those in the larger complexes are more nearly planar degenerate. Provided that a complete LH1 ring consists of 16 $\alpha\beta$-heterodimeric units,[8,9] the isolated complexes studied in this work ($(\alpha\beta)_{4-13}$, ref 4) would correspond to arcs ranging in size from approximately one-quarter of a ring to almost fully circular oligomers. It is clear, however, that the complexes do not contain a collection of identical, noninteracting pigment dimers, since polarization values would have decreased uniformly over the absorption band with increasing oligomerization state, rather than in a wavelength-dependent manner (Figure 1). It has been proposed[18] that a cluster-size dependence of the optical properties, including a shift in the polarization rise from the center to the red wing of the absorption band and a red shift and narrowing of the emission band with increasing size, would arise as a consequence of energy transfer among pigments within inhomogeneous clusters.[46] However, as further discussed below, this effect alone would not readily explain the observed aggregate-size dependence of absorption maximum and bandwidth as the cluster size increased from about 4 to 9 heterodimers (Table 1).

In an alternative model to account for the oligomerization-state dependent optical properties, the LH1 antenna is proposed to consist of a curvilinear array of exciton-coupled transition dipoles. This proposal is based upon the assumption that at low temperature, fluorescence originates predominantly from the lowest excitonic energy level which, as the oligomers increase in size, accounts for a decreasing fraction of the absorption band. Such an arrangement is essentially an extension of the model proposed for the B820 BChl dimer[20,47] and is analogous to the organization postulated for LH1 BChls.[27]

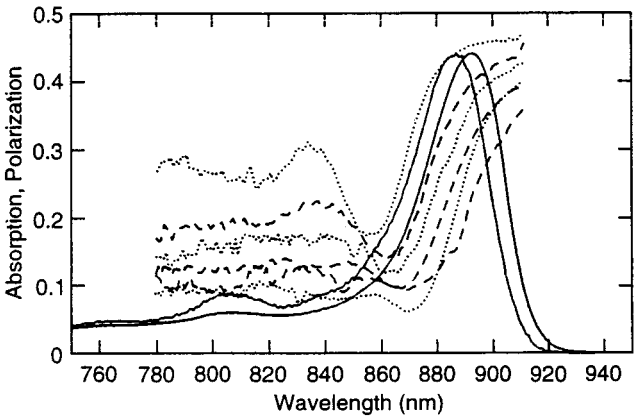

Figure 1. Fractional absorption and fluorescence polarization of LH1 oligomers from *R. sphaeroides* strain M21 at 77 K. Measurements were performed as described elsewhere[3] and are presented in summary form. Fractional absorption ($1-T$) spectra (solid traces) shown for preparations with estimated oligomerization states of ~4 (left) and 11 (right) $\alpha\beta$-heterodimeric units, respectively. Polarization values expressed as: $p = (I_{||} - I_{\perp})/(I_{||} + I_{\perp})$, where $I_{||}$ and $I_{\perp}$ are relative intensities of fluorescence with polarization either parallel or perpendicular, respectively, to polarization direction of excitation light. Detection was at 925 nm; p corrected as described.[3] Fluorescence polarization (dotted and dashed traces) shown (left to right) for preparations with estimated oligomerization states $(\alpha\beta)_{n\pm1}$ for $n = 4$, 5, 6, 7, 9, and 11, respectively.

TABLE 1: Maxima and Bandwidths of Experimental and Calculated Spectra

experimental max λ^a (bandwidth)^b			simulated max λ (bandwidth)		
N^c	absorption	fluorescence	N	absorption	fluorescence
4	886 (440)	903 (430)	4	846 (400)	849 (410)
5	889 (440)	907 (395)	5	847 (395)	850 (405)
7	891 (435)	908 (385)	7	848 (385)	852 (405)
9	892 (420)	908 (355)	10	849 (380)	853 (405)
11	891 (405)	910 (360)	15	849 (370)	854 (400)
M	890 (360)	908 (355)			

^{a} (nm). ^{b} (cm^{-1}). ^{c} N refers to the estimated oligomerization state with M representing the membrane-bound complex (experimental[4]) or to the number of units included in the calculation (simulated). For the latter, the conditions were as in Figure 6E, except that the spectra were convoluted with a triangular slit function, 4 and 12 nm fwhm for absorption and fluorescence, respectively.

Computational Model. To evaluate the effects of both site inhomogeneity and excitonic interactions upon the optical properties of the oligomeric series of complexes, absorption and fluorescence polarization spectra were calculated for different fractions (4 to 15 $\alpha\beta$-heterodimeric units) of a 16-unit circular array. The pigment geometry within a unit was assumed to be identical to that of B850 BChls in the LH2 complex of *R. acidophila*.[48] The *R. rubrum* LH1 projection map[9] was used as a template for their arrangement into a 16-unit structure, which placed the centers of both the α and β BChls on approximately the same circle with radius 46 ± 1 Å, with uncertainty due to limited resolution of the projection map. This resulted in a center−center distance between BChls on adjacent $\alpha\beta$ heterodimers of 8.8 ± 0.4 Å as compared to 8.9 and 8.8 Å in LH2 from *R. acidophila*[32] and *R. molischianum*,[7] respectively, and an intraunit distance of 9.6 Å, compared to 9.6 and 9.2 Å in the two LH2 complexes. Respective values of 9.2 and 9.3 Å for the intra- and interheterodimer Mg−Mg distances of B875

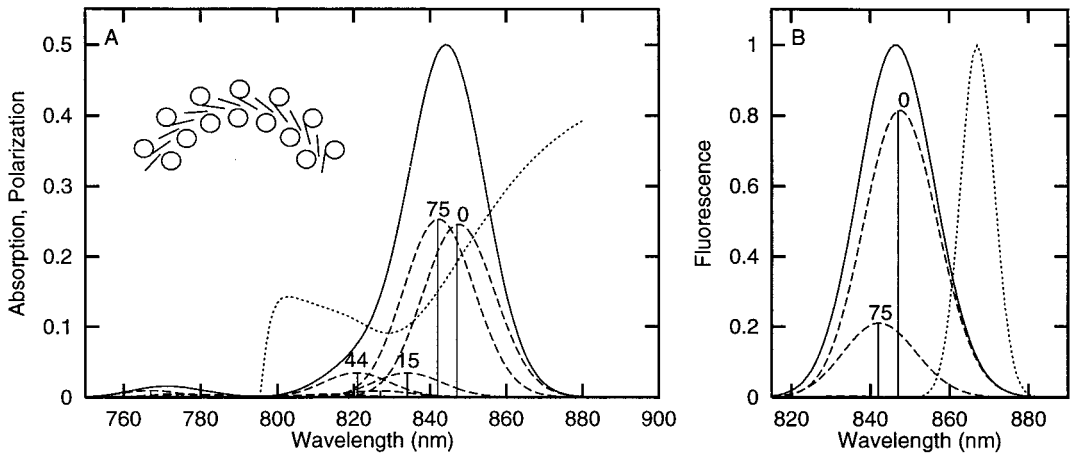

Figure 2. Illustration of calculation methods used in spectral simulations. (A) Calculated absorption and fluorescence polarization spectra. (B) Corresponding fluorescence emission spectrum; optical filter used for emission detection indicated by dotted trace. (A) excitonic components (stick spectra) resulting from interactions between pigments within 7-unit array, arranged as illustrated in the inset, dressed with Gaussian envelopes (dashed, $\Gamma_{hom} = 288$ cm^{-1}) and absorption spectrum obtained by summation (solid); relative angles with lowest energy component are indicated. For emission spectra (B), same components were weighted by a Boltzmann term, accounting for fast thermal equilibration. The polarization spectrum, calculated from relative angles and magnitudes of components in the absorption and emission spectra, is shown in A (dotted trace). V_{intra} and V_{inter} were 262 and 259 cm^{-1}, respectively. Monomer absorptions set at 807 nm, with a random deviation given by an inhomogeneous distribution function with width $\Gamma_{IDF} = 400$ cm^{-1}, corresponding to one of 500 solutions averaged to obtain Figure 5C and D. Absorption and fluorescence emission spectra were normalized to 0.5 and 1.0, respectively.

BChl have been calculated recently for the *R. sphaeroides* LH1 complex,[49] based upon protein structure predictions and the homology to the *R. molischianum* LH2.

Spectral components resulting from excitonic coupling, involving all BChls within a given oligomeric array, were calculated using a point-dipole approximation,[50] taking only the lowest energy (Q_y) transitions into account. The relative interaction energies were determined by the dipole geometries and oscillator strengths, while their absolute values depend on the magnitude of the dielectric constant of the medium. Assuming equal oscillator strengths for both BChls, the described pigment geometry resulted in relative inter- and intraunit interaction energies (V_{inter} and V_{intra}, respectively) that were very nearly the same: $V_{inter}/V_{intra} = 0.99 \pm 12\%$. For comparison, the crystallographic data for *R. acidophila* yielded a ratio (V_{inter}/V_{intra}) of 0.89 for LH2. An estimate for the absolute magnitude of the interaction energies (260 cm^{-1} for V_{intra}) was based upon the optical properties of the B820 complex, proposed to reflect excitonic splitting of the absorption spectrum of a dimer of BChls, each with an average monomer absorption wavelength near 807 nm.[20] By assuming that pigment geometry within the $\alpha\beta$-dimeric unit of the B820 complex is identical to that of B850 BChls of LH2, and using a monomeric dipole strength of 41 Db^2 (ref 51), a relative dielectric constant of 1.4 is obtained. This value is similar to those used by others[37,45] and was generally maintained throughout as the scaling factor for the interaction energies in calculations described below.

To minimize the number of variables, no attempt was made to reproduce the actual absorption and emission maxima by further ad hoc assumptions concerning protein-induced spectral shifts or the homogeneous Stokes shift. This left only the homogeneous monomeric bandwidth (Γ_{hom}, fwhm) and the width of the inhomogeneous distribution function (Γ_{IDF}, fwhm) as variables. Construction of absorption and fluorescence emission, excitation and polarization spectra from stick spectra, representing the calculated spectral composition of a complex, is described in Computation Methods and illustrated in Figure 2.

Oligomer Size Dependence of Absorption Maxima. The relationship between oligomer size and absorption red shift brought about by excitonic coupling is shown in Figure 3. Here,

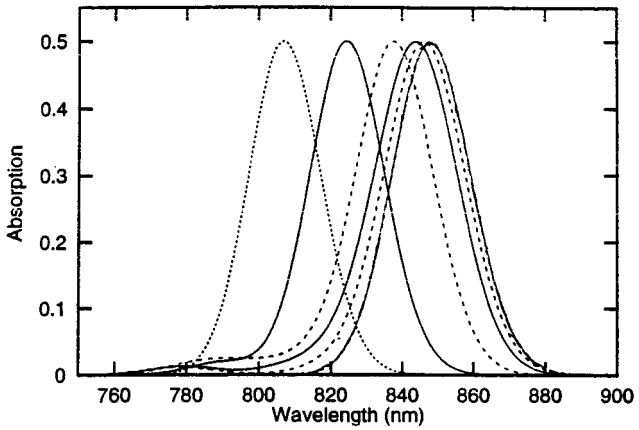

Figure 3. Cluster-size dependence of calculated absorption spectra. Spectra shown are for monomeric BChl (···) and fragments consisting of 1, 2, 4, 8, and 16 (alternatingly — and - - - -) $\alpha\beta$ heterodimers of the same 16-unit circular array, with nearest neighbor geometry as described in text and partly depicted in Figure 2. $\Gamma_{hom} = 360$ cm^{-1}.

inhomogeneous band broadening, which did not significantly alter the absorption maxima (Table 1), was ignored. Absorption maxima for clusters larger than eight units were all red shifted by about 40 nm with respect to the monomeric wavelength. This is slightly more than twice that for single $\alpha\beta$ heterodimers ($\sim$18 nm), in agreement with the numerical solution for the low-energy edge E of the excitonic absorption band of extended linear chromophore aggregates with uniform nearest-neighbor interaction energies V, i.e., $E \approx -2.4V$.[41] Although a cluster-size dependence was still apparent for oligomers of more than four $\alpha\beta$ heterodimers, clearly coupling of only a few dimeric units leads to most of the red shift.

Spectral Properties of Disordered Pigment Arrays. The relative effects of homogeneous and inhomogeneous band broadening on absorption, fluorescence emission, and fluorescence excitation spectra were investigated by numerical calculations for clusters of 5, 8, and 15 dimeric units. Γ_{hom} was varied between 50% and 100% of the overall experimental bandwidth

($\Gamma \approx 360$ cm^{-1}) and Γ_{IDF} was adjusted to yield the same overall absorption bandwidth for the average of 500−2000 individual solutions, about 10 times more than required to smooth out most statistical fluctuations. Results for $\Gamma_{hom} \approx 100\%$, 80%, and 60% of Γ are shown in Figure 4. When the absorption band was solely homogeneously broadened (4A and B), the emission spectra of the clusters were only slightly red shifted relative to their absorption maxima, reflecting that the absorption profiles were made up of just a few, poorly resolved excitonic components (see also Figure 2). Inclusion of some inhomogeneous broadening had two clear effects on the calculated spectra. First, the emission spectra for relatively large clusters showed enhanced red shifts and a small bandwidth reduction. This cluster-size dependence of emission spectra is analogous to that described for the disordered dimer model.[18] Second, with more inhomogeneous aggregates, excitation spectra were red shifted, with respect to the absorption bands, due to the simulated selective detection of fluorescence in the long-wavelength tail, resulting in excitation spectra of a nonrandom subfraction of the array. Especially with smaller clusters, this resulted in distorted bands (4E−F). It is possible that this effect contributed to the observed broadening and 1−2 nm red shifts of the experimental excitation spectra, relative to corresponding absorption bands, ascribed initially to an oligomer-size heterogeneity within each preparation.[3] However, the shifts in experimental excitation spectra were considerably smaller than those shown in Figure 4E, suggesting a lower limit for the homogeneous bandwidth of about 70% of the total width of the absorption band ($\Gamma_{hom} \geq 250$ cm^{-1}).

The cluster-size dependence of the fluorescence polarization spectra was calculated for the same degrees of inhomogeneous broadening (Figure 5). When the band was assumed to be only homogeneously broadened (Figure 5A and B), the main experimental features were reproduced around the absorption band center, but only for relatively small clusters. Considerably better agreement with experimental spectra (Figure 1) was obtained when the inhomogeneous bandwidth was comparable to the homogeneous width (Figure 5C and D), except that calculated polarization values at the blue side of the Q_y band for semicircular arrays were lower and some were negative (discussed below). When the inhomogeneous distribution function considerably exceeded the homogeneous bandwidth (Figure 5E and F), polarization spectra were steeper than observed experimentally. It is therefore concluded that, within the limits of the method used, the best agreement with experimental results is obtained when Γ_{hom} and Γ_{IDF} are taken to be of similar magnitude.

Simulated Optical Properties of the Dimer. The effect of varying the homogeneous bandwidth on the excitation and polarization spectra was also assessed for a single $\alpha\beta$ heterodimer, representing the B820 complex (Figure 6A). The results again show that inhomogeneity produces a red-shifted excitation spectrum due to selective detection of fluorescence from long-wavelength components. In contrast to larger arrays, this is accompanied by a narrowing of the spectrum because the absorption spectrum of disordered dimers is composed of separate low-energy components, rather than of exciton manifolds. Experimental 77 K absorption and (polarized) excitation spectra, detected at 840 nm for B820, indeed exhibit a 5-nm red shift of the latter.[20] On the basis of this value, as well as on the absence of significant narrowing of the excitation spectrum, it is concluded that, also for the single dimeric model, a homogeneous bandwidth of 270−300 cm^{-1} provides the best agreement.

Inclusion of Vibronic Bands. Calculated polarization spectra upon selective long-wavelength detection (Figure 6A) suggest that the width of the inhomogeneously broadened low-energy band does not explain the absence of negative polarization values in the experimental dimer spectra. It is possible that in this region, the presence of (0−1) vibrational transitions, with dipole orientations similar to those in the main (0−0) band, effectively obscure higher energy (0−0) excitonic components with which negative polarization values are associated. In addition, vibronic components in the emission band might moderate the selectivity in the detection. Including a vibronic band in the calculations improved the similarity of the simulated and experimental spectra both for dimers (Figure 6C and D) and for oligomers (Figure 6E and F). Nevertheless, the minima in calculated polarization spectra for aggregates of intermediate size remained lower than those in the experimental ones. A random series of individual solutions indicated that this may result from the possibility that only two or three excitons carry most of the intensity of the Q_y band; consequently, in approximately half-circular arrays, on average, the high and low energy components make a relatively large angle.

Effect of Lowering the Interdimer Coupling Strength. It has been suggested[36] that, because of the van der Waals proximities of BChl macrocycles, the coupling strength within heterodimers is greater than that between chromophores on adjacent subunits. To investigate the relative importance of interdimer interactions for observed spectral properties, V_{inter}/V_{intra} was reduced from 1.0 (Figure 6E and F) to 0.65 and 0.3. A decrease in interdimer coupling strength to less than 100 cm^{-1} resulted in a blue shift and loss of the size dependence of the absorption maxima, corresponding to disordered dimers rather than more delocalized excitons, accompanied by more shallow polarization spectra (not shown). Although for V_{inter} between 130 and 210 cm^{-1} (i.e., about 50% and 80% of V_{intra}, respectively), the minimum values of the polarization spectra were now similar to those seen experimentally, these calculated spectra were still not sufficiently steep. It is concluded that V_{inter} is not much smaller than experimentally derived values for coupling energy within dimeric units (i.e., 200−260 cm^{-1}).

Discussion

Assumptions. The nature of the excited state and the mechanism of intra- and intercomplex energy transfer in light-harvesting complexes depends both on the relative strength of pigment coupling and on the degree of static and dynamic disorder in chromophore site energies. Here, oligomer-size dependence of the optical properties of the LH1 complex at 77 K was simulated by numerical calculations of different degrees of site inhomogeneity. Experimental properties of the B820 complex provided an estimate for the intradimer interaction energy, while the interdimer coupling strength was extrapolated from this value on the basis of structural data for LH2 and LH1.

The first assumption was that pigment−pigment interactions in the antenna complex are sufficiently well characterized by a point-dipole approximation. An extended monopole approach would lead to ~30% lower nearest neighbor interaction energies,[37] which is not expected to qualitatively alter outcomes. The intradimer interactions may have charge-transfer character[36,52] and thus the scaling factor for coupling strength (the reciprocal of the dielectric constant), upon which V_{inter} was based, could have been underestimated. However, similarities of experimental and simulated properties decreased when V_{inter} was reduced to <0.5 V_{intra}, as oligomeric character was lost. With an intradimer interaction energy of 260 cm^{-1}, best

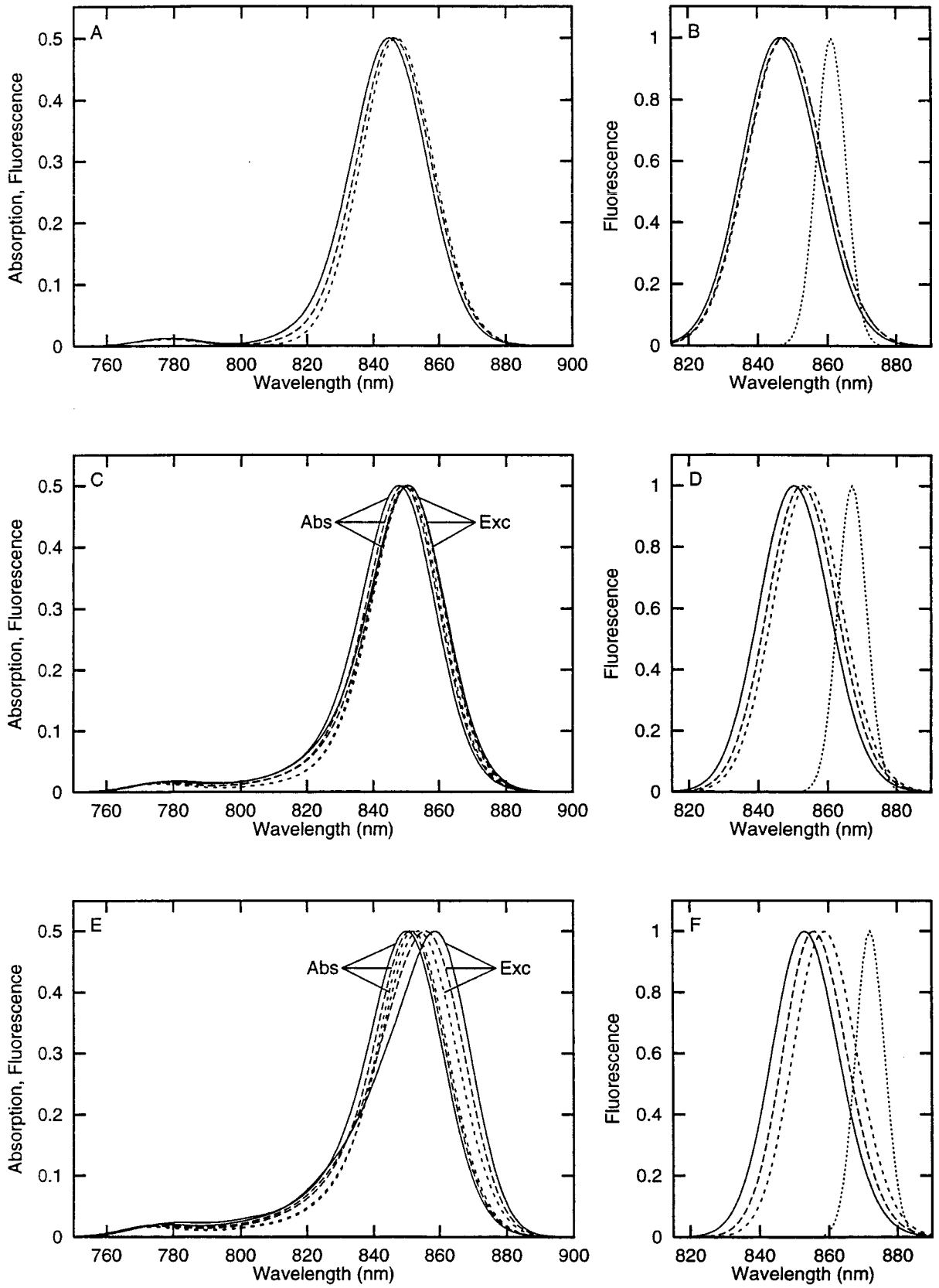

Figure 4. Cluster-size dependence of calculated absorption and fluorescence spectra for different relative contributions of homogeneous and inhomogeneous broadening to the overall bandwidth. (A, C, E) Absorption (Abs) and fluorescence excitation (Exc) spectra; (B, D, F) Fluorescence emission spectra. (A, B) $\Gamma_{hom} = 353$ cm^{-1}, $\Gamma_{IDF} = 0$ cm^{-1}; (C, D) $\Gamma_{hom} = 288$ cm^{-1}, $\Gamma_{IDF} = 400$ cm^{-1}; (E, F) $\Gamma_{hom} = 216$ cm^{-1}, $\Gamma_{IDF} = 550$ cm^{-1}. Each panel shows spectra for fragments of 5 (—), 8 (— —), and (- - -) 15 units of the same array as in Figure 3. Corresponding absorption and excitation spectra coincided in (A) and therefore are not identified separately. Dotted traces (B, D, and F) same as in Figure 2B. (C−F) show the average of 500 solutions.

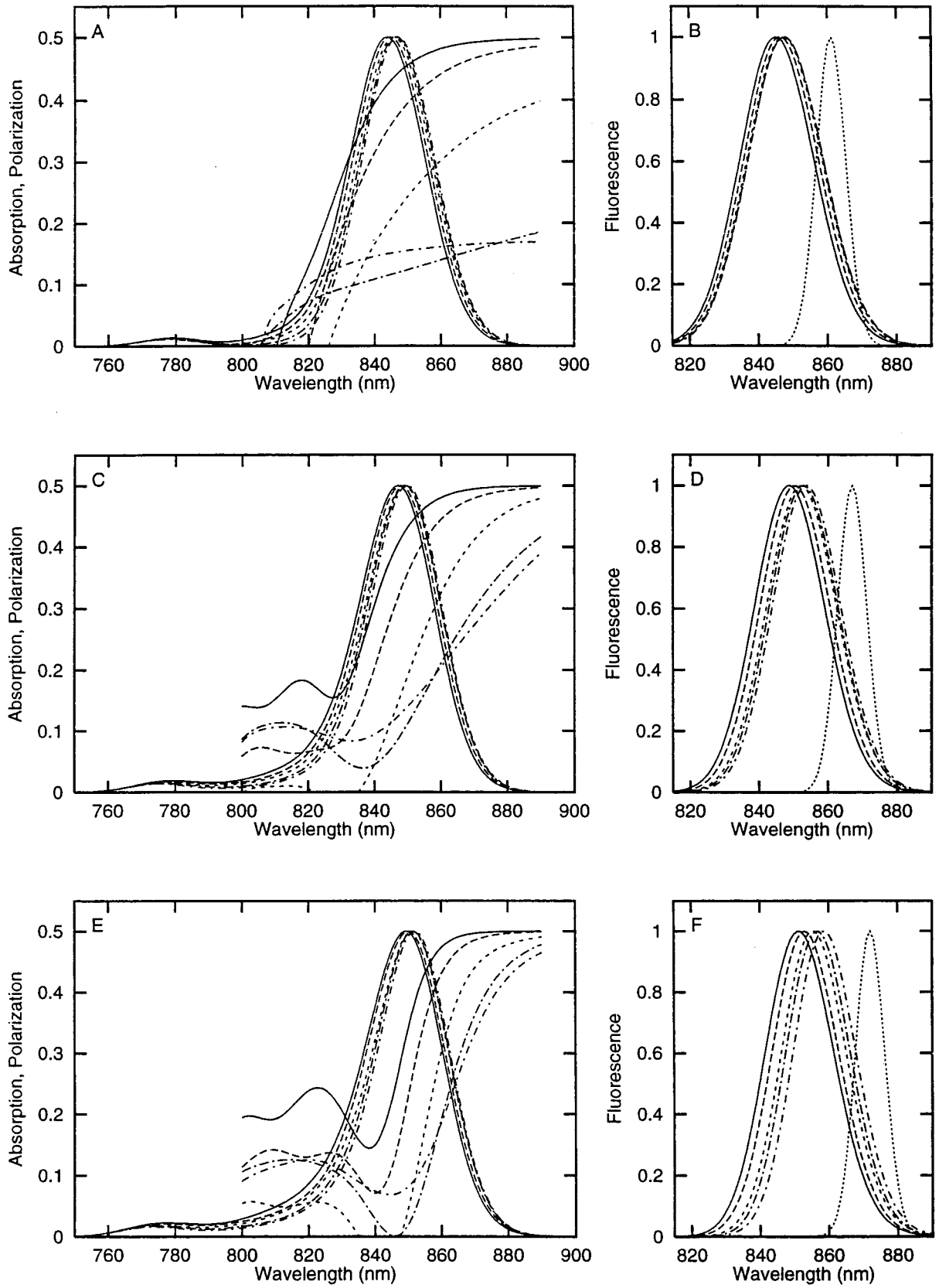

Figure 5. Simulation of array-size dependence of absorption and fluorescence polarization spectra. (A, C, and E) Absorption and fluorescence polarization spectra; (B, D, and F) Fluorescence emission spectra. All conditions the same as for the corresponding panels in Figure 4, except the fragment sizes which in each panel correspond to oligomers of 4 (—), 5 (— —), 7 (- - -), 10 (•—•—•), and 15 (•-•-•) $\alpha\beta$-heterodimeric units.

agreement was obtained with a coupling strength of 200−250 cm^{-1} for pigments on adjacent structural units. These values are comparable to recent estimates[43] from an LH2 CD fit.

A second assumption was that homogeneous exciton bands are approximated by Gaussians. The simulated polarization spectra showed that to obtain satisfactory fits, asymmetry in the form of vibronic components had to be introduced, especially within the blue wing of the absorption band. While the

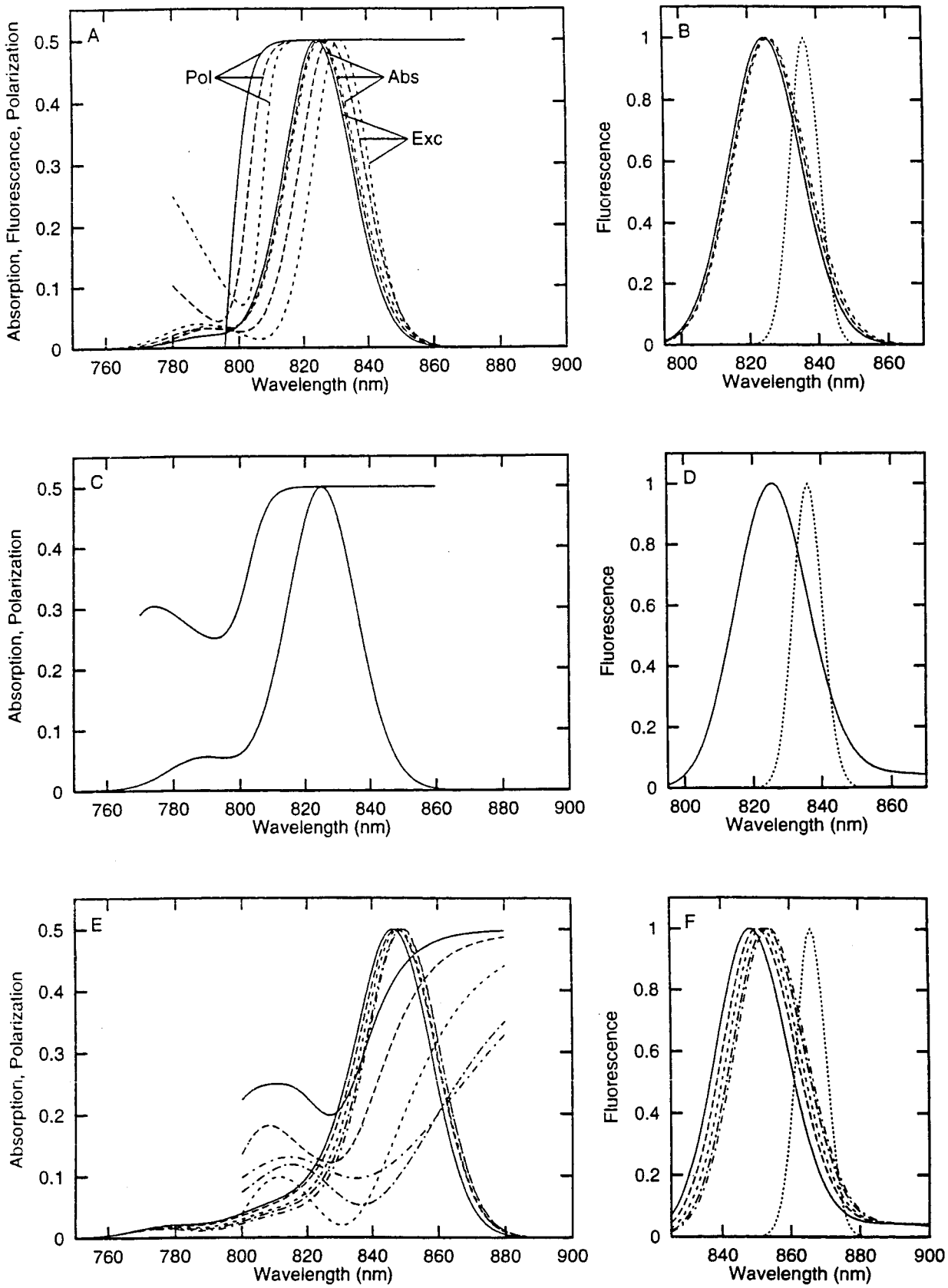

Figure 6. Simulated spectral properties with different Γ_{hom} and Γ_{IDF}, and contribution of vibronic bands. (A) Absorption (Abs), fluorescence excitation (Exc) and polarization (Pol) spectra for a dimer; (B) Fluorescence emission spectra for a dimer. (—), $\Gamma_{hom} = 353$ cm^{-1}, $\Gamma_{IDF} = 0$ cm^{-1}; (− −), $\Gamma_{hom} = 288$ cm^{-1}, $\Gamma_{IDF} = 305$ cm^{-1}; (- - -), $\Gamma_{hom} = 216$ cm^{-1}, $\Gamma_{IDF} = 410$ cm^{-1}. (C) Absorption and polarization for a dimer; (D) Fluorescence emission spectra for a dimer ($\Gamma_{hom} = 288$ cm^{-1}, $\Gamma_{IDF} = 305$ cm^{-1}). (E) Absorption and polarization; (F) Fluorescence emission spectra for same cluster sizes as in Figure 5; $V_{inter}/V_{intra} = 1.0$ and $\Gamma_{hom} = 300$ cm^{-1}, $\Gamma_{IDF} = 375$ cm^{-1}. In panels C−F, a progression of vibronic bands was added to each excitonic component, at 200, 340, 560, and 650 cm^{-1} above (absorption, panels C and E) or below (fluorescence, panels D and F) the (0−0) transition, each with 2% of the intensity of the latter. Dotted traces same as in Figure 2B. Spectra for $\Gamma_{hom} \neq 0$ cm^{-1} are the average of 5000 individual solutions.

homogeneous band shape could have been refined further,[53] attainment of the closest possible agreement between experimental and calculated spectra was not attempted. Assumptions about protein-induced shifts in site energies also were omitted to simplify these simulations and to better identify main trends.

Finally, within the fluorescence lifetime, excitonic band structure was assumed to be stable, with excitation energy rapidly equilibrating over all excitonic components of a single complex. For individual solutions, dipole strengths of main excitonic components, obtained with conditions that best reproduced experimental results ($\Gamma_{hom} \approx 300$ cm^{-1}, $\Gamma_{IDF} = 300-400$ cm^{-1}, $V_{inter} = 200-250$ cm^{-1}), were mostly between 4 and 8 times that of the monomer. This agrees with superradiance measurements, where dipole strengths of the lowest energy component below 100 K were 6−8 times the monomer.[40] The distribution of excitonic components will thus be 2−3 times narrower than Γ_{IDF} (exchange narrowing), i.e., 100−200 cm^{-1} fwhm, the same order of magnitude as the Boltzmann factor at 77 K ($kT \approx 55$ cm^{-1}), justifying the assumption of rapid thermal equilibration. In contrast, at 4 K ($kT \approx 3$ cm^{-1}), slow equilibration phenomena are observed.[17,38,54]

Criteria for Evaluating Simulations. Although red shifts in absorption and emission maxima and polarized excitation spectra shape initially were main criteria used to evaluate simulated spectral properties, it was found that when disorder was increased, the maxima of excitation spectra should also depend on array size (Figure 6). Reexamination of experimental spectra, both for B820[20] and larger LH1 oligomers,[3] showed that a mismatch between absorption and excitation spectra has indeed been observed. The magnitude of this simulated selective detection of long-wavelength fluorescence thus provided another criterion for evaluating simulated spectra.

Size-Dependence of Spectral Red Shifts. The red shift in absorption maximum (807−∼850 nm) as a result of BChl−BChl interactions within nearly fully circular homogeneous arrays (Figure 3) was not significantly affected by disorder, if the width of inhomogeneous distribution did not exceed the coupling energies (Table 1). Greater disorder resulted in slightly enhanced, rather than reduced, red shifts, as well as increased dipole strength near high-energy edges of exciton bands (∼770 nm, Figure 5E), both presumably reflecting monomer character of distribution outliers. A mismatch between centers of the energy distributions of the α and β pigments had a similar effect when exceeding coupling strengths (not shown).

In contrast, absorption depended strongly upon interdimer coupling strength (Figure 6E). A size dependence of absorption maxima (3 nm between $(\alpha\beta)_4$ and $(\alpha\beta)_{15}$) similar to experimental values (4−5 nm between $(\alpha\beta)_4$ and $(\alpha\beta)_{13}$ [3,4]) was only reproduced when V_{inter} was comparable to V_{intra} (Table 1). Agreement was equally close for corresponding emission maxima (4−5 nm simulated, 5−7 nm experimental[3]), which like coupling strengths, are also determined by disorder.[18] Thus, conditions that yielded the best simulation of other optical properties (Figures 5C,D and 6E,F) also nearly reproduced the trend of size dependence of both absorption and emission maxima. Only ∼4 nm of the experimentally observed Stokes shift (∼18 nm) could be ascribed to spectral inhomogeneity, with the remaining 14 nm attributable to a homogeneous Stokes shift of 200 cm^{-1}, about twice that for the B820 dimer.[20] Finally, reductions in overall bandwidths of absorption spectra (as a result of exchange narrowing[41]) and emission spectra (inhomogeneous cluster-size dependence[18]) were also largely reproduced (Table 1).

There remained a considerable difference (∼40 nm) between experimental LH1 absorption maxima and those simulated on the basis of the B820 spectral properties (Table 1). This may be due to further reductions in all site energies by ∼600 cm^{-1}, as a result of changes in the protein environment upon oligomerization of $\alpha\beta(BChl)_2$ units and lowering temperature from 300 to 77 K. It is also possible that this reflects different B820 and LH1 pigment geometry within the dimer. Stark effect spectroscopy has revealed that, unlike B820, LH1 exhibits a large change in polarizability upon excitation. This could reflect an admixture of a charge-transfer state into the lowest excited state of the elementary dimer.[55−58] For the reaction center special pair, this effect contributed strongly to the red shift to 870 nm. Finally, compared to the B820 dimer, oligomerization and cooling of LH1 could result in a slightly altered intradimer pigment geometry,[52] and thus coupling strengths between neighboring chromophores may have been systematically underestimated.

Relative Contributions of Interaction Energy and Disorder. The mismatched maxima of simulated absorption and excitation spectra for long-wavelength fluorescence (Figure 6) provided an upper limit for the degree of disorder (∼450 cm^{-1}), indicating that experimental differences between absorption and excitation spectra for both B820 and LH1 fit an Γ_{IDF} of 300−400 cm^{-1}. The shape of the polarized excitation spectra (Figure 5) demonstrated that without including disorder, realistic simulation was not possible for nearly fully circular arrays, and again suggested that values of 300−400 cm^{-1} provided the best simultaneous fit for array sizes. By introducing asymmetry of homogeneous absorption bands (approximated by a weak vibronic progression) into simulations, the similarity of experimental and calculated polarization spectra was also significantly improved at the high energy side where vibronic absorption dominated (Figure 6E). In contrast, although polarized fluorescence was detected at the low energies, emission at these wavelengths was still dominated by the main component and inclusion of vibronic components in the emission band did not greatly alter simulated spectra.

Regarding whether the approach used here is applicable to sections of a circular model, simulating the removal of a single unit from a full circle results in a gain in strength on the blue side of the absorption band which becomes slightly more asymmetric. Since no neighboring chromophore is available for coupling, average delocalization lengths at the edges are less than elsewhere in the array, where delocalization is limited only by disorder. Thus, excitons associated with these edge pigments are, on average, less red shifted. These considerations also explain spectral differences in strains lacking the Puf X protein in which the LH1 circle is thought to be complete and absorption spectra are more symmetric and red shifted by ∼4 nm.[5]

Conclusions

Neither excitonically coupled homogeneous pigment clusters nor inhomogeneously broadened dimer spectra accounted exclusively for the experimental spectral features. The latter were reproduced by assuming a homogeneous bandwidth between 75 and 90% of overall width and an interdimer coupling strength not much smaller than interactions within dimeric units. Here, the width of the Γ_{IDF} required to account for an overall width of about 360 cm^{-1} was between 300 and 400 cm^{-1}. Together with average interaction energies (200−260 cm^{-1}), this leads to a ratio Γ_{IDF}/V of 1.2−2.0. Similar estimates for disorder and coupling strength have been obtained by absorption, pump−probe,[37−39,59−60] and superradiance[40] measurements which assess nearest neighbor interactions and are more or less

insensitive to chromophore array geometry. While the former provides an upper coupling strength estimate ($<\sim 300$ cm^{-1}), pump−probe absorption difference spectra fitted to temperature-dependent inhomogeneous broadening (200−400 cm^{-1} for LH1 between 4 and 300 K), which when combined, suggest $\Gamma_{IDF}/V \approx 0.65-1.3$. Superradiance reflects average dipole strength of thermally equilibrated exciton manifolds and temperature dependence has yielded a direct estimate for Γ_{IDF}/V of $\sim<1.0$.[40] In contrast, CD, like polarized fluorescence, is sensitive to circular array geometry, although the precise geometrical factors that play a role are different.[61] Both probe interactions across one-quarter of a circle and measure disorder through the effects on pure excitonic states; polarized emission spectroscopy is also sensitive to disorder via energy-selective detection. Γ_{IDF}/V ratios, based on fits to LH2 CD ($\sim$1.8), agree with superradiance which established that for LH2 this ratio (2−3) is temperature-independent and greater than for LH1. Thus, a multitude of spectroscopic properties of LH2 and LH1 can be fitted with a minimal, but robust parameter set. That numerical simulations of optical properties yield consistent estimates for these parameters, demonstrates their validity.

Acknowledgment. This research was supported by the Human Frontier Science Program (W.H.J.W, C.N.H., and R.vG) and U.S. Department of Agriculture Grant 91-01640 (R.A.N.).

References and Notes

(1) van Grondelle R.; Dekker, J. P.; Gillbro, T.; Sundström, V. *Biochim. Biophys. Acta* **1994**, *1187*, 1.

(2) Fleming, G. R.; van Grondelle, R. *Curr. Opin. Struct. Biol.* **1997**, *7*, 738.

(3) Westerhuis, W. H. J.; Niederman, R. A., in preparation.

(4) Westerhuis, W. H. J.; Sturgis, J. N.; Niederman, R. A., in preparation.

(5) Westerhuis, W. H. J.; Farchaus, J. W.; Niederman, R. A. *Photochem. Photobiol.* **1993**, *58*, 460.

(6) McDermott, G.; Prince, S. M.; Freer, A. A.; Hawthornthwaite-Lawless, A. M.; Papiz, M. Z.; Cogdell, R. J.; Isaacs, N. W. *Nature* **1995**, *374*, 517.

(7) Koepke, J.; Hu, X.; Muenke, C.; Schulten, K.; Michel, H. *Structure* **1996**, *4*, 581.

(8) Walz, T.; Jamieson, S. J.; Bowers, C. M.; Bullough, P. A.; Hunter, C. N. *J. Mol. Biol.* **1998**, *282*, 833.

(9) Karrasch, S.; Bullough, P. A.; Ghosh, R. *EMBO J.* **1995**, *14*, 631.

(10) Monshouwer, R.; van Grondelle, R. *Biochim. Biophys. Acta* **1996**, *1275*, 70.

(11) Pullerits, T.; Sundström, V. *Acc. Chem. Res.* **1996**, *29*, 381.

(12) Bolt, J. D.; Hunter; C. N.; Niederman, R. A.; Sauer, K. *Photochem. Photobiol.* **1981**, *34*, 653.

(13) Kramer, H. J. M.; Pennoyer, J. D.; van Grondelle, R.; Westerhuis, W. H. J.; Niederman, R. A.; Amesz, J. *Biochim. Biophys. Acta* **1984**, *767*, 335.

(14) Borisov, A. Y.; Gadonas, R. A.; Danielius, R. V.; Piskarskas, A. S.; Razjivin, A. P. *FEBS Lett.* **1982**, *138*, 25.

(15) van Grondelle, R.; Bergström, H.; Sundström, V.; Gillbro, T. *Biochim. Biophys. Acta* **1987**, *894*, 313.

(16) Bergström, H.; Westerhuis, W. H. J.; Sundström, V.; van Grondelle, R.; Niederman, R. A.; Gillbro, T. *FEBS Lett.* **1988**, *233*, 12.

(17) Timpmann, K.; Freiberg, A.; Godik, V. I. *Chem. Phys. Lett.* **1991**, *182*, 617.

(18) van Mourik, F.; Visschers, R. W.; van Grondelle, R. *Chem. Phys. Lett.* **1992**, *193*, 1.

(19) Parkes-Loach, P. S.; Sprinkle, J. R.; Loach, P. A. *Biochemistry* **1988**, *27*, 2718.

(20) Visschers, R. W.; Chang, M. C.; van Mourik, F., Parkes-Loach, P. S.; Heller, B. A.; Loach, P. A.; van Grondelle, R. *Biochemistry* **1991**, *30*, 5734.

(21) Visschers, R. W.; van Mourik, F.; Monshouwer, R.; van Grondelle, R. *Biochim. Biophys. Acta* **1993**, *1141*, 238.

(22) van Mourik, F.; van der Oord, C. J. R.; Visscher, K. J.; Parkes-Loach, P. S.; Loach, P. A.; Visschers, R. W.; van Grondelle, R. *Biochim. Biophys. Acta* **1991**, *1059*, 111.

(23) van Mourik, F.; Corten, E. P. M.; van Stokkum, I. H. M.; Visschers, R. W.; Loach, P. A.; Kraayenhof, R.; van Grondelle, R. In *Research in Photosynthesis*; Murata, N., Ed.; Kluwer Academic Publishers: Dordrecht, 1992; Vol. 1, p 101.

(24) Reddy, N. R. S.; Picorel, R.; Small, G. J. *J. Phys. Chem.* **1992**, *96*, 6458.

(25) Wu, H.-M.; Reddy, N. R. S.; Small, G. J. *J. Phys. Chem. B* **1997**, *101*, 651.

(26) Wu, H.-M.; Rätsepp, M.; Lee, I.-J.; Cogdell, R. J.; Small, G. J. *J. Phys. Chem. B* **1997**, *101*, 7654.

(27) Novoderezhkin, V. I.; Razjivin, A. P. *FEBS Lett.* **1993**, *330*, 5.

(28) Xiao, W.; Lin, S.; Taguchi, A. K. W.; Woodbury, N. W. *Biochemistry* **1994**, *33*, 8313.

(29) Kennis, J. T. M.; Streltsov, A. M.; Aartsma, T. J.; Nozawa, T.; Amesz, J. *J. Phys. Chem.* **1996**, *100*, 2438.

(30) Leupold, D.; Stiel, H.; Teuchner, K.; Nowak, F.; Sandner, W.; Ücker, B.; Scheer, H. *Phys. Rev. Lett.* **1996**, *77*, 4675.

(31) Sturgis, J. N.; Robert, B. *Photosynth. Res.* **1996**, *50*, 5.

(32) Sauer, K.; Cogdell, R. J.; Prince, S. M.; Freer, A.; Isaacs, N. W.; Scheer, H. *Photochem. Photobiol.* **1996**, *64*, 564.

(33) Fowler, G. J. S.; Sockalingum, G. D.; Robert, B.; Hunter, C. N. *Biochem. J.* **1994**, *299*, 695.

(34) Fowler, G. J. S.; Visschers, R. W.; Grief, G. G.; van Grondelle, R.; Hunter, C. N. *Nature* **1992**, *355*, 848.

(35) Olsen, J. D.; Sockalingum, G. D.; Robert, B.; Hunter, C. N. *Proc. Natl. Acad. Sci. U.S.A.* **1994**, *91*, 7124.

(36) Jimenez, R.; Dikshit, S. N.; Bradforth, S. E.; Fleming, G. R. *J. Phys. Chem.* **1996**, *100*, 6825.

(37) Pullerits, T.; Chachisvilis, M.; Sundström, V. *J. Phys. Chem.* **1996**, *100*, 10787.

(38) Chachisvilis, M.; Kühn, O.; Pullerits, T.; Sundström, V. *J. Phys. Chem. B* **1997**, *101*, 7275.

(39) Kühn, O.; Sundström, V. *J. Chem. Phys.* **1997**, *101*, 4154.

(40) Monshouwer, R.; Abrahamsson, M.; van Mourik, F.; van Grondelle. R. *J. Phys. Chem. B* **1997**, 101, 7241.

(41) Fidder, H.; Knoester, J.; Wiersma, D. A. *J. Chem. Phys.* **1991**, *95*, 7880.

(42) Dracheva, T. V.; Novoderezhkin, V. I.; Razjivin, A. P. *FEBS Lett.* **1996**, *387*, 81.

(43) Koolhaas, M. H. C.; Frese, R. N.; Fowler, G. J. S.; Bibby, T. S.; Georgakopoulou, S.; van der Zwan, G.; Hunter, C. N.; van Grondelle, R. *Biochemistry* **1998**, *37*, 4693.

(44) Alden, R. G.; Johnson, E.; Nagarajan, V.; Parson, W. W.; Law, C. J.; Cogdell, R. J. *J. Phys. Chem. B* **1997**, *101*, 4667.

(45) Koolhaas, M. H. C.; van der Zwan, G.; Frese, R. N.; van Grondelle, R. *J. Phys. Chem. B* **1997**, *101*, 7262.

(46) Visser, H. M.; Somsen, O. J. G.; van Mourik, F.; van Grondelle. R. *J. Phys. Chem. B* **1996**, *100*, 18859.

(47) van Mourik, F.; Visschers, R. W.; Chang, M. C.; Cogdell, R. J.; Sundström, V.; van Grondelle, R. In *Molecular Biology of Membrane-Bound Complexes in Phototrophic Bacteria*; Drews, G., Dawes, E. A., Eds.; Plenum: New York, 1990; p 345.

(48) Freer, A.; Prince, S.; Sauer, K.; Papiz, M.; Hawthornthwaite-Lawless, A.; McDermott, G.; Cogdell, R.; Isaacs, N. W. *Structure* **1996**, *4*, 449.

(49) Hu, X.; Schulten, K. *Biophys. J.* **1998**, *75*, 683.

(50) Scherz, A.; Parson, W. W. *Biochim. Biophys. Acta* **1984**, *766*, 653.

(51) Scherz, A.; Parson, W. W. *Biochim. Biophys. Acta* **1984**, *766*, 666.

(52) Wu, H.-M.; Rätsep, M.; Jankowiak, R.; Cogdell, R. J.; Small, G. J. *J. Phys. Chem. B.* **1998**, *102*, 4023.

(53) Pullerits, T.; Monshouwer, R.; van Mourik, F.; van Grondelle, R. *Chem. Phys.* **1995**, *194*, 395.

(54) Freiberg, A.; Jackson, J. A.; Lin, S.; Woodbury, N. W. *J. Phys. Chem. A* **1998**, *102*, 4372.

(55) Gottfried, D. S.; Stocker, J. W.; Boxer, S. G. *Biochim. Biophys. Acta* **1991**, *1059*, 63.

(56) Beekman, L. M. P.; Steffen, M.; van Stokkum, I. H. M.; Olsen, J. D.; Hunter, C. N.; Boxer, S. G.; van Grondelle, R. *J. Phys. Chem. B* **1997**, *101*, 7284.

(57) Beekman, L. M. P.; Frese, R. N.; Fowler, G. J. S.; Picorel, R.; Cogdell, R. J.; van Stokkum, I. H. M.; Hunter, C. N.; van Grondelle, R. *J. Phys. Chem. B* **1997**, *101*, 7293.

(58) Somsen, O. J. G.; Chernyak, V.; Frese, R. N.; van Grondelle, R.; Mukamel, S. *J. Phys. Chem. B* **1998**, *102*, 8893.

(59) Freiberg, A.; Timpmann, K.; Lin S.; Woodbury, N. W. *J. Phys. Chem. B* **1998**, *102*, 10974.

(60) Nagarajan, V.; Johnson, E. T.; Williams J. C.; Parson, W. W. *J. Phys. Chem. B* **1999**, *103*, 2297.

(61) Pearlstein, R. M. In *Chlorophylls*; Scheer, H., Ed.; CRC Press: Boca Raton, FL, 1991; p 1047.